Plasmodium falciparum LipB mutants display altered redox and carbon metabolism in asexual stages and cannot complete sporogony in Anopheles mosquitoes

Marco Biddau [a,b,*], T.R. Santha Kumar [c], Philipp Henrich [c], Larissa M. Laine [b], Gavin J. Blackburn [d], Achuthanunni Chokkathukalam [d], Tao Li [e], Kim Lee Sim [e], Lewis King [a], Stephen L. Hoffman [e], Michael P. Barrett [a,d], Graham H. Coombs [f], Geoffrey I. McFadden [g], David A. Fidock [c,h,1], Sylke Müller [b,1], Lilach Sheiner [a,b,*]

[a] Wellcome Centre for Integrative Parasitology, University of Glasgow, Glasgow, United Kingdom
[b] Department of Infection, Immunity and Inflammation, University of Glasgow, Glasgow, United Kingdom
[c] Department of Microbiology and Immunology, Columbia University Irving Medical Center, New York, NY 10032, USA
[d] Glasgow Polyomics, Wolfson Wohl Cancer Research Centre, University of Glasgow, Glasgow, United Kingdom
[e] Sanaria Inc., Rockville, MD 20850, USA
[f] Strathclyde Institute of Pharmacy and Biomedical Sciences, University of Strathclyde, Glasgow, United Kingdom
[g] School of Botany, University of Melbourne, Parkville, VIC 3010, Australia
[h] Division of Infectious Diseases, Department of Medicine, Columbia University Irving Medical Center, New York, NY 10032, USA

ARTICLE INFO

ABSTRACT

Malaria is still one of the most important global infectious diseases. Emergence of drug resistance and a shortage of new efficient antimalarials continue to hamper a malaria eradication agenda. Malaria parasites are highly sensitive to changes in the redox environment. Understanding the mechanisms regulating parasite redox could contribute to the design of new drugs. Malaria parasites have a complex network of redox regulatory systems housed in their cytosol, in their mitochondrion and in their plastid (apicoplast). While the roles of enzymes of the thioredoxin and glutathione pathways in parasite survival have been explored, the antioxidant role of α-lipoic acid (LA) produced in the apicoplast has not been tested. To take a first step in teasing a putative role of LA in redox regulation, we analysed a mutant Plasmodium falciparum (3D7 strain) lacking the apicoplast lipoic acid protein ligase B (lipB) known to be depleted of LA. Our results showed a change in expression of redox regulators in the apicoplast and the cytosol. We further detected a change in parasite central carbon metabolism, with lipB deletion resulting in changes to glycolysis and tricarboxylic acid cycle activity. Further, in another Plasmodium cell line (NF54), deletion of lipB impacted development in the mosquito, preventing the detection of infectious sporozoite stages. While it is not clear at this point if the observed phenotypes are linked, these findings flag LA biosynthesis as an important subject for further study in the context of redox regulation in asexual stages, and point to LipB as a potential target for the development of new transmission drugs.

© 2021 The Authors. Published by Elsevier Ltd on behalf of Australian Society for Parasitology. This is an open access article under the CC BY-NC-ND license (http://creativecommons.org/licenses/by-nc-nd/4.0/).

1. Introduction

Malaria remains a tremendous threat to human health with 200 million infections resulting in 405,000 deaths in 2018 (World Health Organization, 2019), so it is imperative that we identify new antimalarial targets. One potential target is the parasite redox regulation system. Plasmodium falciparum is constitutively exposed in all stages of its complex life cycle to molecules that challenge its redox balance. Finding ways to disrupt this delicate balance hold promise for drug development. Indeed, in vitro experiments in which parasites were exposed to exogenous H_2O_2-generating systems proved lethal for intra-erythrocytic stages (Dockrell and Playfair, 1984). Similarly, mature gametocytes are sensitive to the oxidative stress generated by exposure to redox-cyclers

in vitro (Siciliano et al., 2017). Finally, an animal diet that generates an environment rich in reactive oxygen species (ROS) in hepatocytes can reduce *Plasmodium* infection in vivo (Zuzarte-Luís et al., 2017). Despite this importance, and the fact that redox regulation is a fundamental aspect of cellular functions, our understanding of the parasite redox regulatory networks remains limited (Kehr et al., 2010; Müller, 2015).

The apicoplast, a non-photosynthetic plastid acquired via secondary endosymbiosis of a red algal cell, is an active metabolic hub in apicomplexan parasites including *Plasmodium* spp., (Sheiner et al., 2013; Mohring et al., 2014; Frohnecke et al., 2015; Kimata-Ariga et al., 2018; Biddau and Sheiner, 2019). In asexual red blood stages grown in culture, the apicoplast is essential only for the synthesis of isoprenoid precursors (Yeh and DeRisi, 2011). The apicoplast hosts components of the thioredoxin and the glutathione systems, which represent the two best characterised cellular antioxidant systems. Apicoplast-based redox regulators include the peroxiredoxin antioxidant protein (AOP), the dually-targeted (cytosol and apicoplast) enzymes glutathione reductase (GR), and the glutathione peroxidase-like thioredoxin peroxidase (TPx$_{GI}$) (Kehr et al., 2010; Laine et al., 2015). Similarly, two glyoxalase system proteins are apicoplast targeted: glyoxalase-1-like protein (GILP), and glyoxalase 2 (tGloII) (Kehr et al., 2010; Urscher et al., 2010). Glyoxalase 2 is proposed to play a role in the detoxification of incomplete triosephosphate-isomerase reaction products, but is apparently dispensable during intra-erythrocytic development (Wezena et al., 2017). Two additional apicoplast thioredoxin-like proteins (ATrx1 and ATrx2) are found in the peripheral compartments where they play an essential role in the control of protein sorting and folding in response to organelle redox status (Biddau et al., 2018). The *Plasmodium* orthologue of ATrx2 (*Pf*ATrx2; PF3D7_0529100) also appears to be essential (Bushell et al., 2017; Zhang et al., 2018). Many other potential redox-active proteins are predicted to be localised in the apicoplast (Boucher et al., 2018), but their roles are uncharacterized.

An additional molecule proposed to take part in apicoplast redox regulation is α-lipoic acid (LA) (Günther et al., 2007; Frohnecke et al., 2015; Laine et al., 2015). Due to its reducing properties, LA is known as the 'universal antioxidant' (Kagan et al., 1992; Perham, 2000; Goraça et al., 2011; Moura et al., 2015; Tibullo et al., 2017). The proposed antioxidant role of LA in the apicoplast is based on a link between redox regulation and apicoplast pyruvate metabolism via the pyruvate dehydrogenase enzyme complex (PDC). The three enzymes in the PDC complex are pyruvate dehydrogenase (E1), dihydrolipoyl transacetylase (E2) and apicoplast dihydrolipoyl dehydrogenase (aE3). Through a series of reactions, PDC transfers an acetyl group from pyruvate to coenzyme A (CoA) to generate acetyl-CoA for the fatty acid biosynthesis pathway (Mooney et al., 2002; Foth et al., 2005) (Fig. 1). This activity depends on LA bound to the E2 lipoyl domain, which is reduced to dihydrolipoic acid (DHLA) during the process. The final reaction of *Plasmodium* PDC is catalysed by aE3, which re-oxidises DHLA back to LA to allow another cycle of PDC activity (Fig. 1). The activity of aE3 is coupled to the reduction of NAD$^+$ to NADH + H$^+$, which in turn takes part in apicoplast redox regulation (McMillan et al., 2005; Laine, L.M., 2014. Functional, biochemical and structural analyses of *Plasmodium falciparum* pyruvate dehydrogenase complex. PhD Thesis, University of Glasgow. University of Glasgow, UK). The DHLA/LA redox couple has a redox potential of −0.32 V, which is lower than the glutathione/glutathione disulphide (GSH/GSSG) couple potential of −0.24 V, thus making glutathione a potential substrate for DHLA (Packer et al., 1995).

The apicoplast retains its exclusive LA biosynthesis pathway, catalysed by the enzymes octanoyl-ACP:protein *N*-octanoyltransferase (LipB) and lipoyl synthase (LipA) (Fig. 1),

which operates independently from the mitochondrial LA salvage (Crawford et al., 2006; Günther et al., 2009). A *lipB* mutant was earlier generated and shown to have 90% LA depletion (Günther et al., 2007). As a first step to tackle the putative role of LA in redox regulation, we examined the changes in the expression of redox regulation enzymes in this *P. falciparum* mutant (named 3D7$^{\Delta PflipB}$). We also describe the metabolic changes occurring upon *lipB* deletion. As a comparison, we also analysed an aE3 deletion mutant that has only a mild effect on redox balance in the parasite (Laine et al., 2015), potentially because aE3 function might be compensated by alternative apicoplast enzymatic systems coupled to NAD(P)$^+$ reduction such as the NADP$^+$-specific glutamate dehydrogenase (Zocher et al., 2012). Our results describe a correlation between LA availability and redox regulation. Additionally, *lipB* deletion led to changes in central carbon metabolism. Finally, *lipB* deletion, generated in a separate NF54 line, hampers the ability of the parasites to develop in the mosquito, suggesting that LipB is essential in this life stage.

2. Materials and methods

2.1. Parasite culture and assessment of growth

2.1.1. Plasmodium falciparum culturing and synchronisation

Plasmodium falciparum 3D7 parasites (isolated in the Netherlands) were cultured in RPMI 1640 (Invitrogen, UK) supplemented with 11 mM D-Glucose (Sigma Aldrich, UK), 0.5% w/v AlbuMAX II (Invitrogen, UK), 200 mM hypoxanthine (Sigma Aldrich, UK), and 20 mg/ml of gentamycin (PAA, Germany) in human erythrocytes at 5% haematocrit (Trager and Jensen, 1976). Parasites were cultured, maintaining a reduced oxygen atmosphere (1% O$_2$, 3% CO$_2$ and 96% N$_2$) and a constant temperature of 37 °C (referred to as standard procedures). Parasitemias were determined by microscopy-based analysis of Giemsa-stained thin smears and synchronisations were performed following the sorbitol procedure (Lambros and Vanderberg, 1979). Tighter synchronisation was obtained by a combination of sorbitol treatment with magnetic-activated cell sorting (MACS) using LD columns (Miltenyi Biotech, Germany). Briefly, sorbitol-synchronised parasites were maintained in culture until they reached the early ring stage. Cultures were synchronised twice with sorbitol 6 h apart and then cultured until they reached the late schizont stage. Schizonts were purified over a MACS column once cultures had reached a schizont:ring ratio of 1:2. Schizonts were then placed in culture for 1 h with gentle shaking and cultures were synchronised again using the sorbitol method to obtain highly synchronous ring stages with 1 h synchrony. Highly synchronous parasites were used for all time point experiments and RNA extractions, with triplicate cultures for each condition.

2.1.2. Spent medium metabolite quantification

Analyses of D-glucose and L-lactate concentrations from spent culture medium samples were performed using the D-Glucose-HK and L-Lactic acid kits from Megazyme (Ireland) following the manufacturer's protocol. Briefly, parasite cultures for each condition were synchronised using a double sorbitol treatment (Lambros and Vanderberg, 1979) with a 6 h window, and split into triplicate cultures at the same parasitemia. At each time point, an aliquot of the culture was collected from each condition and erythrocytes were pelleted by centrifuging at 1000g for 5 min. The resulting supernatant was then stored at −20 °C. For the enzymatic assay, parasite spent medium samples were diluted by 1:6 with double distilled water.
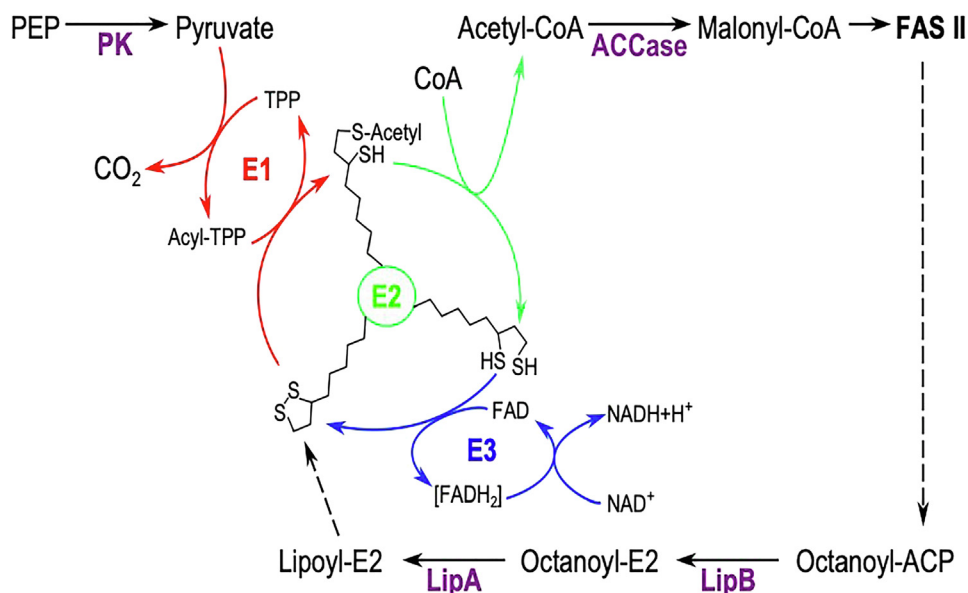
Fig. 1. Schematic representation of Pyruvate Dehydrogenase Complex (PDC) and Lipoic Acid (LA) biosynthesis components and function in the *Plasmodium falciparum* apicoplast. Each of the PDC enzyme reactions is shown in a different colour (E1, red; E2, green; E3, blue). The three states of E2-conjugated LA are depicted onto the schematic E2. ACCase, acetyl-CoA carboxylase; CoA, coenzyme A; FAD, flavin adenine dinucleotide; FAS II, fatty acid biosynthesis type II; LipA, lipoyl synthase; LipB, Octanoyl-ACP: protein *N*-octanoyltransferase; NAD, nicotinamide adenine dinucleotide; PK, pyruvate kinase; TPP, thiamine pyrophosphate. (For interpretation of the references to colour in this figure legend, the reader is referred to the web version of this article.)

2.2. Evaluation of antioxidant gene expression

2.2.1. Reverse-Transcription quantitative PCR (RT-qPCR)

Highly synchronous parasites (see section 2.1.1) were cultured in triplicate for each condition until they reached 26, 30 and 34 h post-invasion (pi). Pellets of infected red blood cells (RBCs) at 6–8% parasitemias were then washed three times in PBS and kept at −80 °C. Nucleic acids were extracted using the RNeasy kit (QIAGEN). Contaminating DNA was removed using the Turbo DNA-free kit (Thermo Fisher Scientific). RNA samples were then reverse transcribed using the RETRO-script kit (Thermo Fisher Scientific). Quantitative PCR (qPCR) was performed using the Power SYBR Green Master Mix (Thermo Fisher Scientific, UK) adding 20 ng of cDNA for each reaction and 300 nM of each primer (see Supplementary Table S1). All reactions were run in a 7500 Real-Time PCR System (Applied Biosystems, UK). The calculation of relative gene expression was performed using the $\Delta\Delta(Ct)$ method (Livak and Schmittgen, 2001).

2.2.2. Protein extraction and quantitative fluorescent western blot

For protein extraction, saponin-lysed parasite pellets were resuspended in 2D lysis buffer (100 mM Hepes pH 7.4, 5 mM MgCl2, 10 mM EDTA, 0.5% (v/v) Triton X-100, 5 μg/ml of RNase A, 1× complete protease inhibitor cocktail (Roche, Switzerland) in double distilled (dd)H2O). Samples were subjected to three rounds of freezing and thawing on dry ice, and incubated at 4 °C for 5 min in a sonicated water bath. Samples were then centrifuged at 13,000g for 20 min at 4 °C. Supernatants containing protein fractions were quantified using the Protein Assay kit (Bio-Rad, UK), with BSA used to generate a reference quantification curve.

Western blot analysis was performed by separating 20 μg of protein sample by SDS-PAGE with NuPage Novex 4–12% and 15% (w/v) Bis-Tris gels (Invitrogen, UK). Separated proteins were transferred to Protran nitrocellulose membranes (Schleicher & Schuell, Germany) using a Transblot semi-dry transfer system (Bio-Rad, UK). Membranes were blocked with 5% (w/v) dried skimmed milk in PBS for 1–18 h and incubated for 1 h with two or more primary antibodies. Primary antibodies used for relative quantification

included *P. falciparum* rabbit anti-actin antibody (1:12,000, loading control), *P. falciparum* rabbit anti-1-CysPx (1-Cys peroxiredoxin) antibody 1:50,000; *P. falciparum* rabbit anti-2-CysPx (2-Cys peroxiredoxin) antibody at 1:70,000; *P. falciparum* rabbit anti-BCKDH E2 antibody at 1:5000; *P. falciparum* rabbit anti-isocitrate dehydrogenase antibody at 1:10,000 and *P. falciparum* rabbit anti-PDC E2 lipoyl domain antibody at 1:250. Membranes were washed three times in PBS containing 0.2% (v/v) Tween 20 and 2.5% (w/v) dried skimmed milk. Blots were then probed with infrared dye-conjugated antibody (1:10,000, IRDye800CW goat anti-rabbit antibody; LI-COR Biosciences, USA) for 1 h and washed again twice. Membranes were loaded in an Odyssey SA scanner (LI-COR Biosciences, USA) and fluorescent signal intensities quantified with the Image Studio software (LI-COR Biosciences, USA). All antibodies were custom made by Eurogentec.

2.3. Metabolomics experiment and analysis

2.3.1. ¹³C-U-D-glucose labelling experiment setup

Parasites were cultured until parasitemias attained 6–8%. Two sorbitol treatments were performed at approximately 8 and 14 h pi. After synchronisation, triplicate parasite cultures were initiated using a medium where D-glucose was replaced with ^{13}C-U-D-glucose (99%, CK Gas Products Ltd, UK) and the haematocrit was set to 1%. A control culture of uninfected RBCs was prepared with the same conditions. All cultures were incubated for 20 h following standard procedures until late trophozoites. At this point, parasite culture metabolism was rapidly quenched at 4 °C in a bath of dry ice and 70% ethanol (Vincent and Barrett, 2015). Erythrocyte pellets were then obtained and washed in ice-cold PBS by centrifugation at 800g for 5 min at 4 °C. Infected RBCs in the pellets were enriched using MACS LD column purification (Miltenyi Biotech, Germany) and a QuadroMACS magnet (Miltenyi Biotech, Germany) with all steps performed at 4 °C. Enriched samples were quantified using a Neubauer cell counting chamber and a Scepter 2.0 Handheld Automated Cell Counter (Millipore) to have 2.0×10^8 infected RBCs per sample. The same number of uninfected RBCs was collected as a control. All the samples were then added to a solution

of HPLC-grade chloroform:methanol:water (1:3:1; v/v/v), at a concentration of 2×10^8 parasites per 0.5 mL solution, incubated in ice in a sonicating water bath for 2 min and extracted for 1 h at 4 °C and 1500 rpm on an orbital shaker. After extraction, samples were centrifuged at 13,000g for 20 min at 4 °C, and supernatants transferred into glass mass spectrometry vials (Thermo Fisher Scientific, UK) and stored at −80 °C until LC-MS analysis.

2.3.2. LC-MS analyses

Metabolomics analyses were performed by LC-MS using an Ultimate 3000 LC system (Dionex, UK) connected to a Q Exactive HF Hybrid Quadrupole-Orbitrap mass spectrometer, (Thermo Fisher Scientific). The system was controlled by the software Chromeleon (Dionex, UK) and Xcalibur (Thermo Scientific), acquiring both positive and negative ionisation modes. Chromatographic separation was performed with a ZIC-pHILIC chromatography column (150 mm (length) × 4.6 mm (diameter) 5um (bead size) ; Sequant, Uemå, Sweden) using a two solvent system consisting of solvent A: 20 mM ammonium carbonate and solvent B: acetonitrile (Table 1).

2.3.3. Metabolomic data analysis

Vendor-specific raw data were initially centroided and converted into the open format mzXML for subsequent processing. PeakML files (Scheltema et al., 2011) were then generated by extracting the chromatographic peaks contained in the mzXML files using the detection algorithm from XCMS (Tautenhahn et al., 2008). The data processing pipeline mzMatch.R (Jankevics et al., 2012) was used to sort and combine all PeakML files corresponding to replicates and to exclude all non-reproducible data. Further steps of noise-filtering, gap-filling, and metabolite identification were performed on PeakML files utilising data obtained from metabolic standards run in parallel. For each metabolite of interest, the proportions of each isotopologue and its relative abundance in the sample were determined. The PeakML.Isotope.TargetedIsotopes function of mzMatch-ISO (Chokkathukalam et al., 2013) was used to scan the PeakML files for labelled metabolite quality and quantity. All metabolites of interest in this study were reliably identified by comparison of the chromatographic retention times and the m/z values with an authentic metabolic standard processed in parallel. These should be then considered as "identified compounds" or level 1 according to the Metabolomic Standard Initiative (Sumner et al., 2007). All metabolomics data was corrected for natural carbon isotope abundance and reagent impurity using the software IsoCor (Millard et al., 2019).

2.4. Double cross-over deletion of PfLipB in the NF54 strain by the Cre-loxP system

Plasmodium falciparum NF54 parasites were cultured in complete medium containing RPMI 1640 salts and 10% heat-inactivated human serum (Graves et al., 1984). The strategy for deleting *pflipB* using *Cre-lox*P is depicted in Supplementary Fig. S1. Briefly, we employed a double crossover recombination strategy to generate parasite lines lacking a functional *pflipB* locus (PlasmoDB ID: PF3D7_0823600). A 0.5 kb fragment of *pflipB*, PCR-amplified from NF54 genomic DNA using primers p1/p2 (Supplementary Table S1), was cloned into PCC1-*cdup*-h*dhfr*-DXO between the *Sac*II and *Afl*II sites and served as the homology region for the first cross-over (O'Neill et al., 2011). The second homologous fragment (0.5 kb) was PCR-amplified using primers p3/p4 and cloned between *Eco*RI and *Avr*II sites to give rise to an 8.5 kb PCC1-*cdup*-h*dhfr*-Δ*lipB* plasmid. Fifty μg of this plasmid was used to transfect NF54 parasites by electroporation and transformed parasites were selected with 1.5 nM WR99210. Drug pressure was maintained for 7 days and parasites were then cultured in drug-free medium up to day 27 when WR99210-resistant parasites appeared. Resistant

Table 1
Percentage of solvent A and B used over time to perform LC-MS.

Solvent A (%)	Solvent B (%)	Time (min)
20	80	0
80	20	30
95	5	31
95	5	35
20	80	36
20	80	46

parasites were then treated with 1.0 μM 5-Fluorocytosine (in DMSO) to remove single crossover-integrated plasmid and episomal forms, both of which contain the *cdup* negative selection marker (Maier et al., 2006). PTET-BSD-*Cre* (a kind gift from Alan Cowman, Walter and Eliza Hall Institute, Australia) was transfected into recombinant NF54 parasites and cultured in 2.5 μM blasticidin S-hydrochloride for 7 days, after which single-cell cloning was performed (Goodyer and Taraschi, 1997).

2.5. Generation of Pf ΔlipB gametocytes and production of salivary gland sporozoites

Gametocytes were induced from *Pf∆lipB* and wild-type (WT) NF54 parasite lines by multiple rounds of sub-culturing for 14–18 days with nutrient deprivation, as described (Ponnudurai et al., 1986). Gametocyte induction and maturation was monitored microscopically by Giemsa-stained thin blood smears from culture samples. Mature gametocyte pellets were mixed with fresh O-type Rh$^+$ blood and human serum to produce an artificial blood meal at approximately 50% hematocrit for mosquito feeds. The final concentration of stage V gametocytes in artificial blood meals was 1.0%±0.1% (mean ± S.E.M. across seven experiments), which was equivalent to the gametocyte numbers observed with NF54 parasites (Supplementary Table S1). *Anopheles stephensi* mosquitoes were fed 3–5 days after their emergence from pupae. Fed mosquitoes were maintained for 13–16 days before recovery of salivary gland sporozoites (SPZ) by hand dissection.

2.6. Ultrastructural analysis of midgut oocysts

The infected midgut oocysts were fixed in 4%/0.1% formaldehyde/glutaraldehyde and immersed in a 50:50 glycerol/water solution for Differential Interference Contrast (DIC) imaging. Using a Nikon Ti Eclipse inverted microscope, cut midgut sections were pre-screened for the presence of oocysts at 10× magnification using an automated tiling feature of the Nikon NIS Elements 3.2 software. Individual oocysts were imaged at high magnification using a 60 × NA 1.4 oil immersion objective with a matching DIC slider. Images were compiled using the National Institute of Health (USA) ImageJ program (https://imagej.nih.gov/ij).

Morphology of developing oocysts was examined by fixing dissected mosquito midguts in 2.5% glutaraldehyde in PBS, and then in 0.5% OsO$_4$, dehydration in an ethanol series, embedding in London Resin White, and semi-thin sections (400 nm) were mounted on glass slides and stained with 0.5% toluidine blue (w/v): 0.1% Na$_2$CO$_3$ (w/v) for 10 s, and then imaged on an Olympus BH-2 light microscope.

3. Results

3.1. Deletion of lipB results in accelerated differentiation and changes in apicoplast and cytosol antioxidant levels

Pronounced LA deficiency was previously detected in the trophozoite stage in *lipB* knockout (KO) line 3D7$^{\Delta PflipB}$ parasites (Günther et al., 2007). The LA depletion seen in this mutant

provided an opportunity to take the first steps to investigate whether this deficiency affected the apicoplast antioxidant composition. We monitored the relative transcription levels of genes encoding apicoplast antioxidants at 26, 30 and 34 h pi by qPCR for both 3D7$^{\Delta PflipB}$ and the parental (3D7^{WT}) parasites. We used primer sets to specifically quantify the transcripts of the apicoplast redox-active proteins TPx$_{GI}$ (PF3D7_1212000), ATrx2 (PF3D7_0529100) and AOP (PF3D7_0729200) (Fig. 2A), which take part in the thioredoxin redox system, and the apicoplast glyoxalase system proteins GILP (PF3D7_0604700) and tGlo (PF3D7_1205700) (Supplementary Fig. S2). Among these, TPx$_{GI}$ had the largest change in expression levels, with relative transcription levels displaying three to four-fold increases at 30 h pi and 34 h pi compared with 3D7^{WT}. Similarly, ATrx2 relative expression showed a four-fold increase compared with the 3D7^{WT} parasites at 26 h pi followed by a two-fold decrease at 34 h pi, when AOP also showed a two-fold decrease (Fig. 2A). In contrast, the apicoplast glyoxalase system enzymes presented no significant differences in relative expression (Supplementary Fig. S2).

In light of these observed changes in apicoplast antioxidant expression, we wanted to test whether the cytosolic antioxidant composition was also affected. Therefore, we used quantitative fluorescent western blotting to monitor the relative levels of GST (PF3D7_1419300), 1CysPx (PF3D7_0802200) and 2-CysPx (PF3D7_1438900). These proteins were measured in 3D7$^{\Delta PflipB}$ and 3D7^{WT} late trophozoites at 34 h pi. We observed a significant two-fold increase in protein levels for GST and 1-CysPx in 3D7$^{\Delta PflipB}$ mutants (Fig. 2B, Supplementary Fig. S3). Conversely, 2-CysPx levels appeared to remain unchanged between the two lines (Fig. 2B).

In a previous study, *lipB* deletion was reported to result in a slight increase in parasite growth in culture (Günther et al., 2007). We examined the effect on asexual cycle progression in more detail and found that at 30 h pi the 3D7$^{\Delta PflipB}$ mutant showed an increase in differentiation into schizonts with a 6 h advance compared with 3D7^{WT} (Fig. 2C). This accelerated differentiation resulted in faster completion of the trophozoite stage and of the whole asexual cycle but had no effect on the average number of merozoites (Fig. 2D).

These finding provide indirect evidence of a change in the underlying redox potential of both the apicoplast and the cytosol upon *lipB* deletion at the time points examined. It remains to be determined whether the redox changes observed occur as a result of the shorter differentiation window or are the cause for it. The detection of some changes in redox regulators starting at 26 h pi, 4 h prior to the observed accelerated differentiation, suggests the latter.

3.2. Deletion of lipB affects parasite carbon metabolism

In eukaryotic cells, the compartmental redox state and the availability of redox conducting and regulating molecules in different cellular compartments are intertwined with the activity of metabolic pathways. The redox conditions in a cellular compartment affect the function of its metabolic enzymes, while in turn, the metabolic reactions in a compartment generate metabolites that impact its redox state. Thus, we proceeded to examine whether the observed redox changes in 3D7$^{\Delta PflipB}$ mutants coincide with changes in central carbon metabolism. We chose to make this analysis alongside a *P. falciparum* apicoplast dihydrolipoamide dehydrogenase (aE3) knock-out mutant (3D7$^{\Delta Pfae3}$) (Laine et al., 2015). Unlike 3D7$^{\Delta PflipB}$, the deletion of a PDC component in 3D7$^{\Delta Pfae3}$ does not result in disruption of LA biosynthesis nor of PDC activity, and its effect on the expression of redox regulators is only mild (Laine et al., 2015), which makes 3D7$^{\Delta Pfae3}$ a relevant negative control.
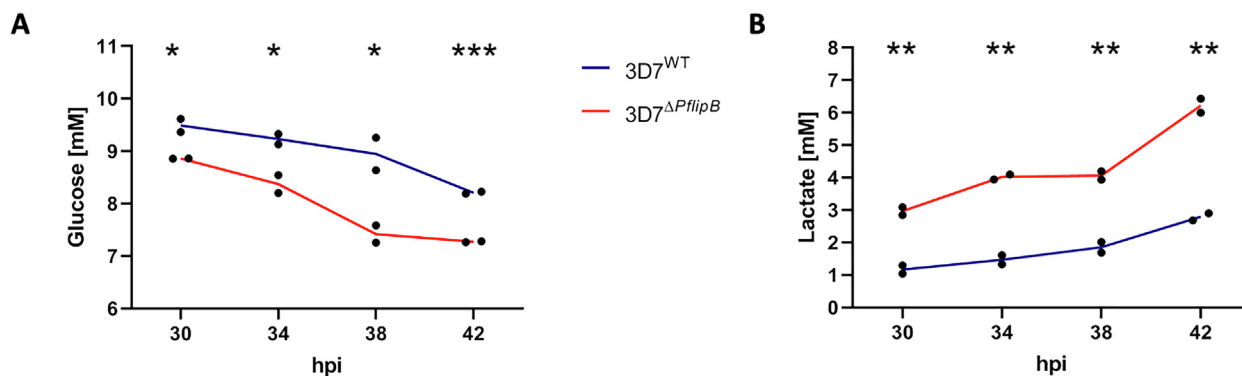
The levels of D-glucose and L-lactate in spent medium were monitored using commercial enzymatic assays in two independent experiments. As glycolytic activity in *P. falciparum* typically peaks during intra-erythrocytic trophozoite development (Shivapurkar et al., 2018), we collected samples at 30, 34, 38 and 42 h pi to cover this developmental stage. Results showed that spent medium samples from 3D7$^{\Delta PflipB}$ contained significantly less D-glucose (Fig. 3A) and more L-lactate (Fig. 3B) than 3D7^{WT} at 42 h pi. Conversely, 3D7$^{\Delta Pfae3}$ mutants did not present this trend and the concentrations for these metabolites in spent medium were comparable to the WT controls (Supplementary Fig. S4).

We further hypothesised that the up-regulation of glycolysis and the change to antioxidant expression described above might affect downstream metabolism and especially the tricarboxylic acid (TCA) cycle. Therefore, we proceeded to set up two steady-state targeted metabolomics experiments in technical triplicates, using the isotope-labelled nutrient ^{13}C-U-D-glucose. 3D7$^{\Delta PflipB}$ and 3D7^{WT} parasites were synchronised and metabolically labelled for 28 h. Parasites at the late trophozoite stage were then rapidly chilled, and the extracted metabolites analysed by LC-MS to follow [^{13}C] labelling. In agreement with the observation from the spent medium, 3D7$^{\Delta PflipB}$ mutants displayed a two-fold increase in the relative levels of the glycolytic metabolite pyruvate and of glycerol-3-phosphate, which derive from a glycolytic intermediate (Fig. 4A, Ba). A similar trend was also displayed by the metabolites 2-oxoglutarate and succinate associated with the TCA cycle, as well as the amino acid aspartate, whereas alanine showed a reduction in relative intracellular level (Fig. 4A, B). The analysis of the labelled fraction for these metabolites showed an immediate conversion of glucose into glycolytic intermediates (Supplementary Fig. S5), in line with previous analyses (Storm et al., 2014). Conversely, the analysis of 3D7$^{\Delta Pfae3}$ mutants showed no significant differences in the relative abundances for these metabolites (Fig. 4C).

Only a small fraction of [^{13}C] labelled triose phosphates was fed into the TCA cycle intermediates in all three parasite lines (Supplementary Fig. S5), as has been well established in the literature (MacRae et al., 2013; Storm et al., 2014; Ke et al., 2015). Interestingly, whereas the 3D7^{WT} control had M + 4, M + 5 and M + 6 citrate labelling, indicative of a complete TCA cycle activity, this was not the case for 3D7$^{\Delta PflipB}$. Rather, in 3D7$^{\Delta PflipB}$ signals for M + 4 and M + 6 citrate were below the detection level, while the M + 5 fraction was significantly decreased (Fig. 4D). In both the experiments an increment of M + 2 citrate was detected for 3D7$^{\Delta PflipB}$ mutants compared with 3D7^{WT}, however, with high variability between the two experiments (Fig. 4D). These changes were not observed for 3D7$^{\Delta Pfae3}$ mutants (Fig. 4E). In the 3D7$^{\Delta PflipB}$ mutant, the presence of M + 2 label in citrate suggests an unchanged flux of glycolytic pyruvate into the TCA cycle. Conversely, the absence of M + 4 and M + 6 citrate isotopologues might lead to a non-cyclic activity of the cycle, unlike that seen in 3D7^{WT} and 3D7$^{\Delta Pfae3}$. These observations are similar to the phenotype found upon deletion of aconitase reported within a study that provided a detailed analysis of the *P. falciparum* TCA cycle (Ke et al., 2015). The significant reduction in the M + 5 citrate fraction could be interpreted as a reduction in carbon fixation activity by the PEP carboxylase branch. This observation is also supported by a decrease in M + 3 labelling for the metabolites malate and fumarate (Fig. 4D). Conversely, no variations in malate and fumarate labelling were observed in the 3D7$^{\Delta Pfae3}$ mutants. To further investigate these variations in the TCA cycle activity in 3D7$^{\Delta PflipB}$, we performed quantitative western blot analysis of the enzymes operating the first steps of the TCA cycle. Interestingly, the 3D7$^{\Delta PflipB}$ mutant up-regulated the branched-chain α-keto acid dehydrogenase (BCKDH) component E2, the first enzyme converting pyruvate to acetyl-CoA (Oppenheim et al., 2014), while its apicoplast parallel PDC E2 displayed no significant difference in abundance (Fig. 5A,
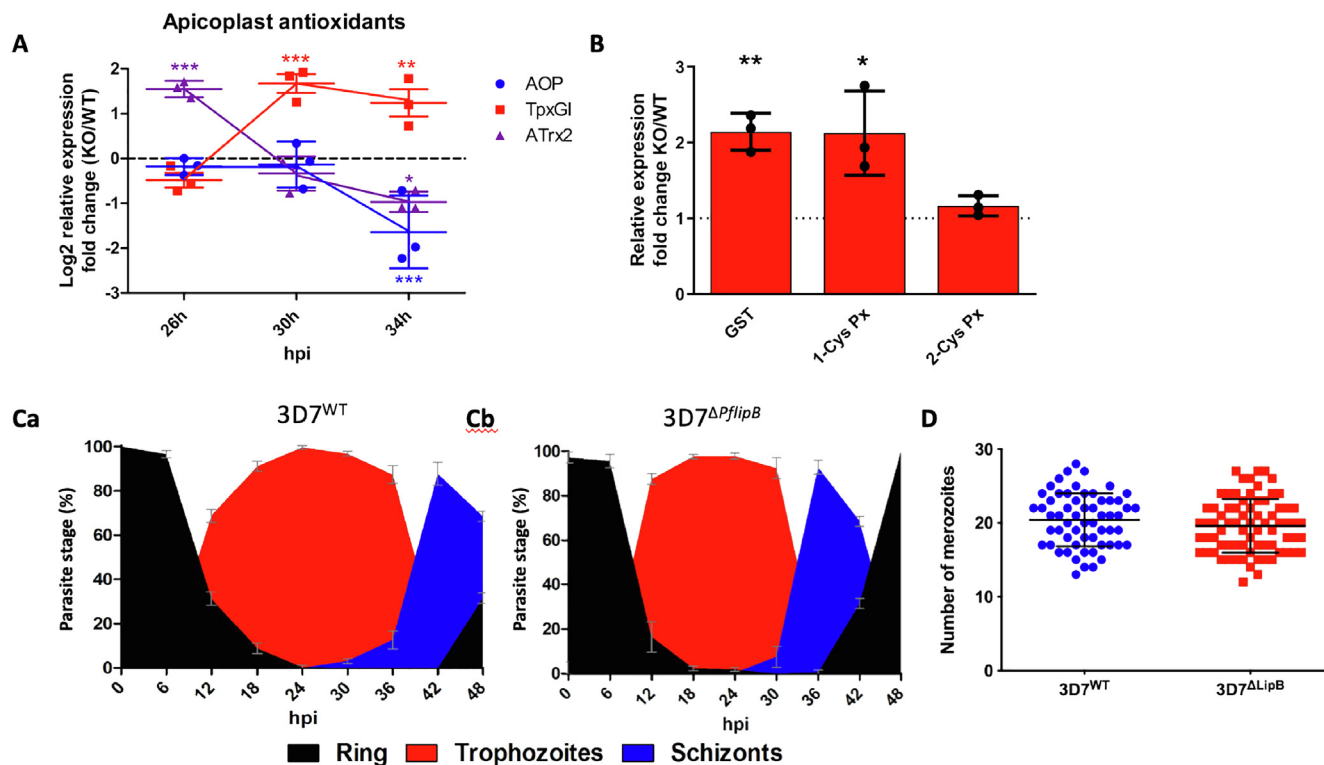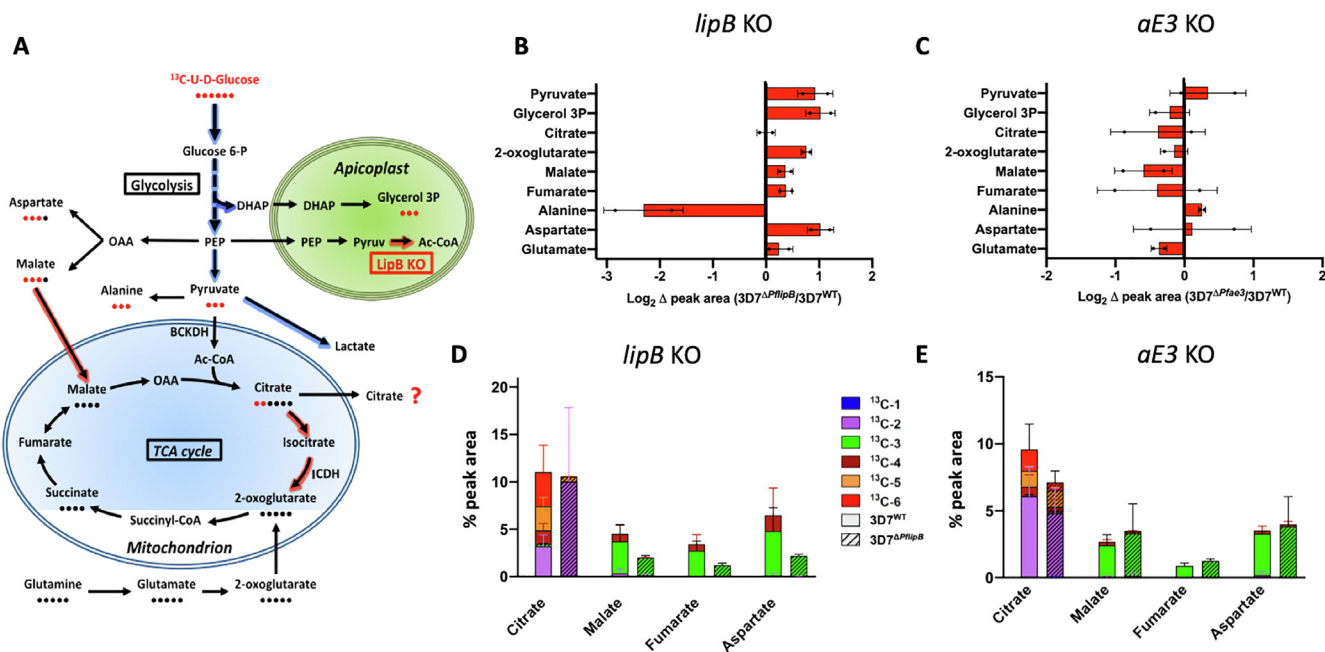
Fig. 2. Analysis of *Plasmodium falciparum* apicoplast antioxidant relative expression levels and cytosolic antioxidant relative protein levels. (A) Relative transcript levels for apicoplast antioxidant protein (AOP), glutathione peroxidase-like thioredoxin peroxidase (TPx$_{Gl}$), and apicoplast thioredoxin-like protein 2 (ATrx2), in the lipoic acid protein ligase B (LipB) mutant compared with wild type. Parasites were highly synchronised following the sorbitol and magnetic activated cell sorting (MACS) protocol (see section 2) and harvested at 26, 30 and 34 h post-invasion (hpi). Differences are expressed as Log$_2$ of the 3D7$^{\Delta PflipB}$/3D7^{WT} ratio of the mean signals from three experiments performed in triplicate (n = 3). Error bars show S.D. Variances were analysed using the two-way ANOVA test coupled with the Bonferroni test using GraphPad Prism 8. Asterisks and graph lines are colour coded as shown in the legend. *P < 0.05; **P < 0.01; ***P < 0.001. (B) Relative protein levels for the cytosolic antioxidant proteins GST, 1-Cys peroxiredoxin (1-CysPx) and 2-Cys peroxiredoxin (2-CysPx). Three independent experiments were performed in technical triplicates and the means (n = 2) of actin-normalised fluorescent signals for each protein were calculated using quantitative fluorescent western blotting. The bars represent the 3D7$^{\Delta PflipB}$/3D7^{WT} average ratio ± S.D. The variance was analysed with the Student's t-test using GraphPad Prism 8. *P < 0.01. KO, knockout; WT, wild type. (C) The variation for each parasite stage during asexual development was estimated by counting 200 random infected red blood cells (RBCs) for each time point for 3D7^{WT} (a) and 3D7$^{\Delta PflipB}$ mutants (b). Fractions are presented as the mean percentage from three cultures for each condition; error bars correspond to S.D. (D) The graph represents the number of merozoites per 'segmenter' stage (n = 100) in 3D7$^{\Delta PflipB}$ mutants and 3D7^{WT}. Bars represent mean ± S.D.

Fig. 3. Analysis of D-glucose (A) and L-lactate (B) in spent medium samples from *Plasmodium falciparum* 3D7$^{\Delta PflipB}$ mutant and 3D7^{WT} parasite cultures. Spent medium samples were collected at 30, 34, 38 and 42 h post-invasion (hpi) and analysed using a commercial enzymatic assay for D-glucose and L-lactate. Triplicate cultures at 2% parasitemia were used for each parasite line for this experiment. The mean signals from two independent experiments (n = 2) are represented by dots in each time point. The variance between the lines at each time point was analysed with the Student's t-test using GraphPad Prism 8. *P < 0.05; **P < 0.01; ***P < 0.001.

Supplementary Fig. S6). Additionally, isocitrate dehydrogenase (ICDH), which operates three steps downstream in the TCA cycle, displayed no differences in abundance compared with 3D7^{WT} (Fig. 5A, Supplementary Fig. S6). These variations in enzyme expression require further analysis. In light of the described

increased glycolytic activity, an up-regulation of BCKDH might be required to sustain the flux of acetyl-CoA in the TCA cycle. The unaltered levels of ICDH contrast with the possible reduced conversion of isocitrate to 2-oxoglutarate in 3D7$^{\Delta PflipB}$, suggested by the observed variations in citrate labelling (Fig. 4D).

Fig. 4. Metabolomic analyses of *Plasmodium falciparum* 3D7$^{\Delta PflipB}$ mutant and 3D7^{WT} parasites using ^{13}C-U-D-glucose labelling. Results from two independent targeted metabolomics experiments in technical triplicates comparing 3D7$^{\Delta PflipB}$ mutants and 3D7^{WT} after incubation in culture medium containing 100% ^{13}C-U-D-glucose for 28 h. (A) Schematics of the *P. falciparum* central carbon metabolism pathways analysed here, highlighting the metabolic adaptations in 3D7$^{\Delta PflipB}$ mutant compared with wild-type (WT) parasites. Arrows shaded in red and blue, respectively, correspond to a decrease and increase in flux for each specific reaction. Red and black dots under metabolite names, respectively, depict the number of labelled and unlabelled carbons, based on the most abundant labelled form of the metabolite. The relative abundances of BCKDH, ICDH and PDC E2 are reported next to each reaction. Ac-CoA, acetyl-CoA; BCKDH, branched-chain ketoacid dehydrogenase; DHAP, dihydroxyacetone phosphate; OAA, oxaloacetate; PEP, phospho*enol*pyruvate. (B,C) Relative intracellular levels for each metabolite obtained by the sum of all the peak areas for each isotopologue of a specific metabolite. The differences in abundance for each metabolite are expressed as Log$_2$ of the 3D7$^{\Delta PflipB}$/3D7^{WT} (B) or Log$_2$(3D7$^{\Delta Pfae3}$/3D7^{WT}) (C) mean ratio ± S.D. (n = 2). (D,E) Bar graphs summarising the percentage of isotopic incorporation in each identified metabolite calculated from the chromatographic peak areas. The bars are divided to represent the mean contribution (n = 2) of the different isotopologues to each metabolite labelled fraction and error bars are S.D. Empty bars represent metabolites identified in 3D7^{WT} parasites, while dashed bars correspond to metabolites from 3D7$^{\Delta PflipB}$ mutants (D) or 3D7$^{\Delta Pfae3}$ mutants (E). The variance in the citrate M + 5 fraction between mutants and 3D7^{WT} is depicted by an asterisk coloured with the corresponding legend colour and was analysed with the Student's *t*-test using GraphPad Prism 8. *P < 0.05.

Lastly, we tested cofactors involved in carbon and energy metabolism, where we observed a decrease in relative intracellular levels of ATP in 3D7$^{\Delta PflipB}$ parasites, while all other cofactors tested were unchanged (Fig. 5B). In addition, 3D7$^{\Delta PflipB}$ mutants had an increase in the ADP M + 5 fraction (Fig. 5C). These results might suggest an increased ATP demand in the mutants, possibly linked to the accelerated differentiation (Fig. 2C), although this explanation remains to be demonstrated directly. In summary, the analysis of 3D7$^{\Delta PflipB}$ mutant metabolism reveals an effect on the activity of both glycolysis and the TCA cycle. The specificity of this phenotype compared with 3D7$^{\Delta Pfae3}$ metabolism (Fig. 4Bb, Cb) provide indirect support to the possibility that there is a link between LA depletion and the observed changes.

3.3. A LipB mutant cannot complete development in a mosquito

We further investigated the development *of lipB*-deleted parasites in mosquitoes. For this analysis, a second *lipB* deletion line was generated by double-crossover gene deletion (Supplementary Fig. S1) in the NF54 background (NF54$^{\Delta PflipB}$), which is superior to 3D7 parasites in its ability to infect mosquitoes. Parasites were maintained in media containing 10% human serum, with the aim of them retaining their capacity to form mature gametocytes. The deletion of *lipB* did not appear to overtly influence sexual commitment in the parasites and mature gametocytes developed as in NF54^{WT} (Table 2, Fig. 6). This allowed us to proceed to evaluate parasite development in the mosquito. Seven mosquito infection experiments were performed with NF54$^{\Delta PflipB}$ gametocytes (Table 2). While midgut oocysts were detectable in all experiments

(Table 2), no sporozoites were detected in any of the infected mosquitoes in any of the seven experiments, while an average of 136,922 ± 17,717 sporozoites were detected in four mosquito infection experiments performed with the parental NF54 (Table 2, Fig. 6). These data indicated a major defect in development in the mosquito in the NF54$^{\Delta PflipB}$ parasites. To explore this further, we examined the morphology of the midgut oocysts, and found that the NF54$^{\Delta PflipB}$ oocysts present an unusual morphology (Fig. 7), which may be suggestive of an attenuated sexual development for this line that could not complete its transmission cycle in the *Anopheles* vector.

4. Discussion

The cellular redox balance of *Plasmodium* parasites is constantly under threat of oxidative stress generated by the metabolic functions of the parasite and by the metabolic activities and defence mechanisms of the host (Becker et al., 2004; Nepveu and Turrini, 2013; Patzewitz et al., 2013; Müller, 2015). Apicoplast-specific redox balance is an integral part of the overall cellular redox steady-state (Kehr et al., 2010; Mohring et al., 2017; Biddau et al., 2018). While fragmented information is available about the different apicoplast redox control pathways, their importance is evident in the series of specific antioxidant systems it hosts (Kehr et al., 2010) and in the redox regulators controlling its biogenesis (Biddau et al., 2018). Similarly, apicoplast-hosted pathways are coupled to redox reactions, including the biosynthesis of isoprenoid precursors, which is coupled to the reduction of NADP$^+$ to NADPH plus H$^+$ (Seeber et al., 2005; Seeber and Soldati-Favre,
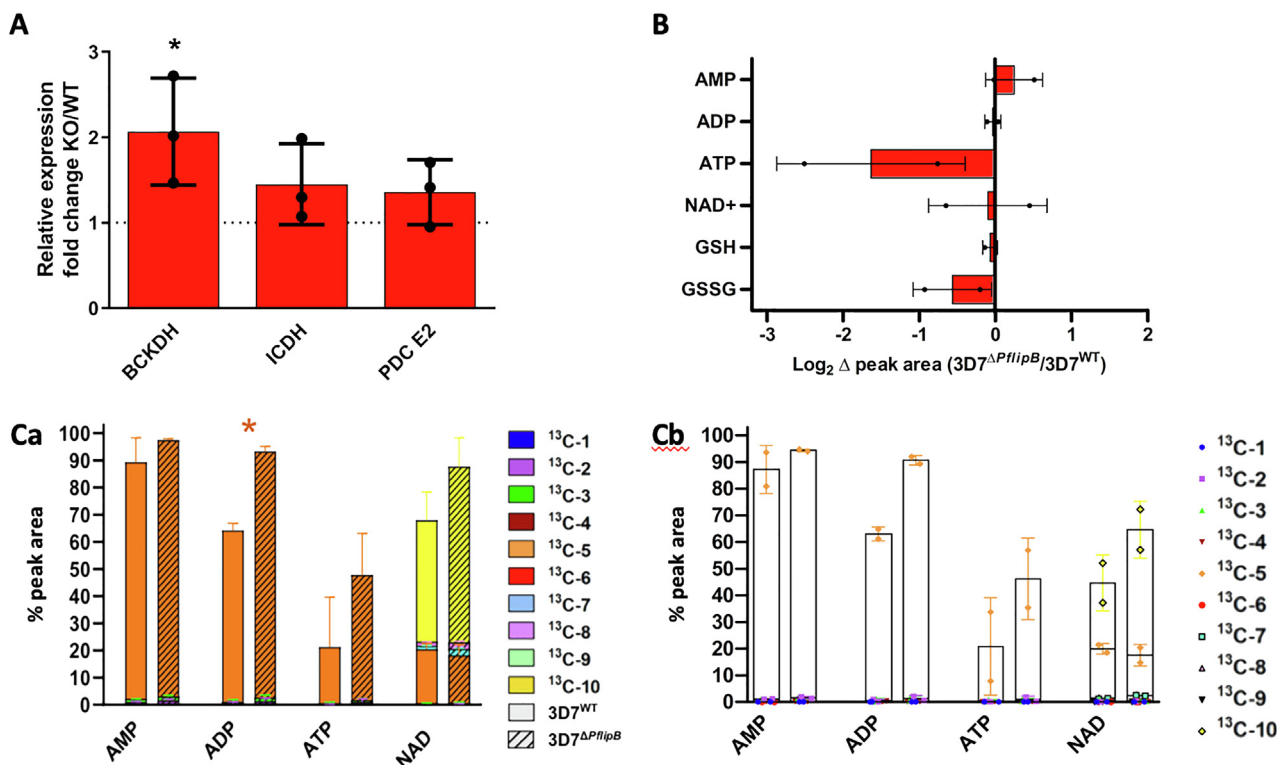
Fig. 5. Analysis of the expression of metabolic enzymes and the levels of cofactors involved in glycolysis and in the tricarboxylic acid (TCA) cycle of *Plasmodium falciparum*. (A) Relative protein levels for the mitochondrial enzymes branched-chain ketoacid dehydrogenase (BCKDH E2), isocitrate dehydrogenase (ICDH) and of the apicoplast enzyme dihydrolipoamide transacetylase (PDC E2). Data from three experiments performed in biological triplicates ($n = 3$) are shown as the $3D7^{\Delta PflipB}$: $3D7^{WT}$ ratio of the actin-normalised mean fluorescent signals for each protein. Error bars represent S.D. The variance was analysed with the Student's t-test using GraphPad Prism 5. *$P < 0.05$. (B) Relative intracellular levels of metabolic cofactors are represented as Log_2 of the $3D7^{\Delta PflipB}$: $3D7^{WT}$ ratio of the means from two experiments in biological triplicates. The relative mean levels are the sum of all peak areas relative to each isotopologue of each metabolite ($n = 2$). Error bars represent S.D. (C) (a) Bar graph summarising the percentage of isotope incorporation in the identified cofactors AMP, ADP, ATP and NAD^+. Data correspond to two experiments performed in biological triplicates ($n = 2$). The bars are divided to the mean contribution of each isotopologue to the total labelled fraction and displays error bars correspond to S.D. Empty bars correspond to metabolites identified in $3D7^{WT}$ parasites, while dashed bars refer to metabolites from $3D7^{\Delta PflipB}$ mutants. The variance of each isotopologue fraction between $3D7^{\Delta PflipB}$ and $3D7^{WT}$ ($n = 2$) is indicated by the asterisk symbol (coloured according to legend) and was analysed with the Student's t-test using GraphPad Prism 8;.*$P < 0.05$. (b) the same graph as (a) is shown with data points indicated for M + 5 (orange) and M + 10 (yellow).

Table 2
Summary of mosquito infection attempts with *Plasmodium falciparum* cell line NF54$^{\Delta PflipB}$.

Stage V gametocytemia in cultures		Final concentration of stage V gametocytemia in the infectious blood meals		Wet mount exflagellation of infectious blood meal per field (x40 phase contrast)		Oocysts/mosquito		Sporozoites/mosquito	
NF54	NF54 LipB KO	NF54	NF54 LipB KO	NF54	NF54 LipB KO	NF54	NF54 LipB KO	NF54	NF54 LipB KO*
0.40%	1.62%	0.11%	0.11%	5.2	11.7	50	32	106,543	0
1.37%	0.63%	0.12%	0.12%	8.1	6.3	36	62	150,178	0
1.45%	0.75%	0.11%	0.11%	9.3	4.9			180,991	0
0.92%	0.93%	0.10%	0.10%	1.9	2.7			109,975	0
	0.87%		0.10%		9.4		28		0
	1.10%		0.12%		5		36		0
	1.03%		0.12%		5.6		53		0
1.04% ± 0.24%	0.99% ± 0.12%	0.11% ± 0.004%	0.11% ± 0.003%	6.1 ± 1.7	6.5 ± 1.2	43.0 ± 7.0	42.2 ± 6.5	136,922 ± 17,717	0 ± 0

Each row represents a separate experiment, with parental NF54 included in the first four.
Despite equivalent numbers of mature gametocytes and rates of exflagellation of male gametes in comparison with parental NF54 parasites, the LipB knockout (KO) parasites failed to produce any salivary gland sporozoites, as determined from dissection and counting of 20 infected *Anopheles* mosquitoes per parasite line per experiment. The bottom row shows composite mean ± S.E.M. data.

2010), and the activity of PDC as discussed here (Fig. 1). LA is proposed to contribute to redox regulation in other systems (Tibullo et al., 2017). The results presented here describing the phenotypes of *lipB* deletion provides preliminary evidence in support of this role within the apicoplast of *Plasmodium*, albeit indirect.

LA is a powerful antioxidant with low redox potential (Packer et al., 1995; Bilska and Włodek, 2005), which prompted us to test how interfering with LA biosynthesis affected apicoplast redox regulation. As a means to address this question, and in the absence of a method to directly and specifically deplete LA from the
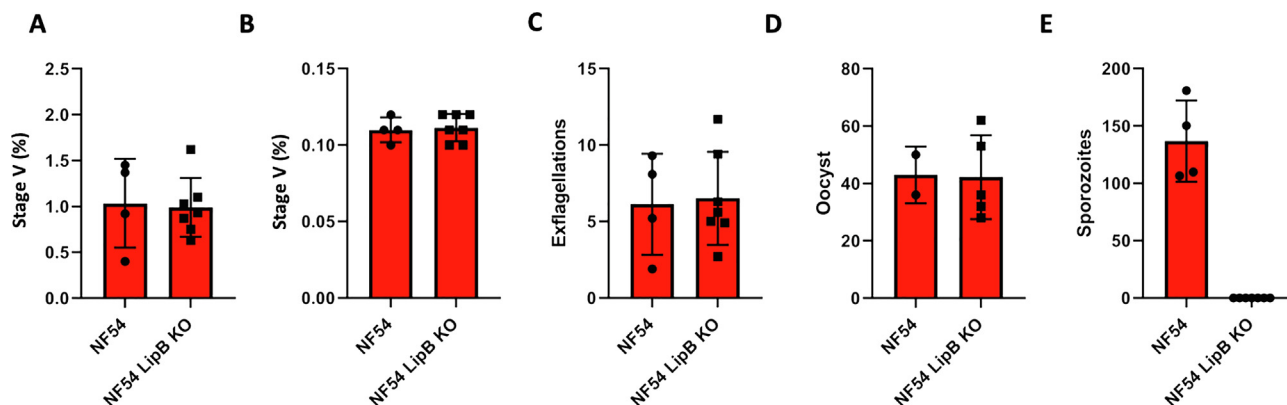
Fig. 6. Bar graphs representing the data from Table 2. All data points are showed as dots for each bar. Error bars correspond to S.D.

apicoplast, we examined the phenotypes of a *lipB* deletion mutant (3D7$^{\Delta PflipB}$) where 90% reduction of LA was earlier reported (Günther et al., 2007). We detected transcriptional changes of the apicoplast redox enzymes peroxidase-like enzyme TPx$_{GI}$, thioredoxin ATrx2, and the peroxiredoxin AOP (Fig. 2A). We cannot exclude that these observations are a result of other outcomes of *lipB* deletion not related to LA depletion. Nevertheless, we propose the hypothesis that the observed redox changes might promote apicoplast redox homeostasis in response to an oxidative stress that may be caused by the depletion of the LA antioxidant function. In support of this hypothesis, up-regulation of TPx$_{GI}$ also occurs in response to other oxidative stresses in *P. falciparum* (Akide-Ndunge et al., 2009). Similarly, we recently reported that the ortholog of *Pf*ATrx2 in the related parasite *Toxoplasma gondii* (*Tg*ATrx2) controls apicoplast gene expression, likely via a redox state-controlled interaction with proteins in transit to the apicoplast lumen (Biddau et al., 2018). If *Pf*ATrx2 performs a similar function, then the changes in its expression in 3D7$^{\Delta PflipB}$ may serve to control protein transit to the apicoplast lumen in response to organelle redox imbalance. The different roles of TPx$_{GI}$ and ATrx2 may account for the different pattern in their transcriptional changes. This proposed putative role for LipB and, potentially, for LA synthesis, in the maintenance of apicoplast redox balance raises the possibility, while speculative, that the apicoplast *Pf*PDC E2 enzyme may operate as an apicoplast antioxidant through its prosthetic LA. Examples of DHLA acting as an electron donor to both GSH and thioredoxin systems have been previously described in other organisms (Packer et al., 1995). DHLA bound to PDC-E2 and to α-ketoglutarate dehydrogenase (KGDH) acts as an electron donor to glutaredoxins in an *Escherichia coli* mutant where both the thioredoxin and the GSH systems were disrupted (Feeney et al., 2011). Similarly, *Mycobacterium tuberculosis* KGDH E2 uses DHLA to transfer electrons received from E3 to peroxiredoxins and contributes to antioxidant defence (Bryk et al., 2002). Additionally, KADH E2-mediated reduction of thioredoxins was observed in mammals (Bunik and Follmann, 1993). A similar redox regulatory role of the apicoplast PDC E2 may explain why it is expressed during the intra-erythrocytic stages (Foth et al., 2005; McMillan et al., 2005), despite the dispensability of fatty acid biosynthesis in this stage (Vaughan et al., 2009). Our attempts to delete PDC E2 in *P. falciparum* using gene replacement were unsuccessful (data not shown), raising the possibility that its role during intra-erythrocytic development is essential. In agreement with this observation, *Pfpdce2* was proposed to be essential during intra-erythrocytic development in a recent whole-genome random mutagenesis screen for *P. falciparum* (Zhang et al., 2018), however, *Pbpdce2*, was not found to be essential in a genome-wide screen performed for *Plasmodium berghei* (Bushell et al., 2017). This hypo-

thetical role for *lipB*, and potentially LA, in redox regulation raises questions about the sources of electrons for LA/DHLA recycling. This might not be attributed exclusively to the flux of glycolytic pyruvate to PDC as this was suggested to contribute to a build-up of acetyl-CoA in the organelle (Lim and McFadden, 2010). A possible alternative candidate for LA/DHLA recycling might be the apicoplast-targeted GSH reductase (GR) (Müller, 2015). The GR-mediated reduction of LA was demonstrated in rats and, in particular, the use of NADPH + H$^+$ as an electron donor was described in mitochondrial fractions (Pick et al., 1995; Haramaki et al., 1997).

Our data identified changes in cytosolic antioxidant expression in 3D7$^{\Delta PflipB}$ parasites. Both enzymes for which we observed upregulation, GST and 1-CysPx (Fig. 2B), are highly abundant in the *P. falciparum* cytosol (Liebau et al., 2002), and both have demonstrated antioxidant activity in this compartment (Krnajski et al., 2001; Harwaldt et al., 2002; Liebau et al., 2002; Deponte and Becker, 2005). One potential explanation for this phenotype might be that a plastid-to-cytosol redox signalling, such as the signalling described in plant chloroplasts and cytosols (reviewed in Dietz et al., 2016) might also exist in *Plasmodium*. Testing this possibility will require further experimentation. In *Arabidopsis thaliana*, chloroplast-originated H$_2$O$_2$ signal induces upregulation of the expression of genes encoding different GSTs as well as enzymes involved in glycolysis and the pentose phosphate pathway (PPP) (Sewelam et al., 2014). Moreover, chloroplast-originated ROS signalling induces changes in the cell cycle progression (Bode et al., 2016).

The hypothesis that plastid-to-cytosol redox signalling occurs in *Plasmodium* is an exciting one which we think the field should consider in future work. Nevertheless, it is important to notice that while generating *lipB* deletion mutants, the parasites were forced through an intense selection bottleneck, and it is not possible to exclude that the observed redox changes may have resulted from adaptation that could have occurred during this process. In the future, it would be interesting to explore this hypothesis further using conditional mutants that would circumvent this complication and that may allow a temporal control of LA depletion.

Because we wanted to examine metabolic changes that might be linked to redox changes, we compared the metabolites between two mutants of the apicoplast PDH complex that show strong (*lipB* our study) or mild (aE3, (Laine et al., 2015)) changes in the expression of redox regulators. Metabolic analysis of 3D7$^{\Delta PflipB}$ mutants highlighted increased glycolytic activity, which is the main energy releasing pathway in blood stage *P. falciparum* (Salcedo-Sora et al., 2014). Increased glycolytic activity in the 3D7$^{\Delta PflipB}$ mutant was mostly evident through increased glucose demand and increased lactate production via spent medium analysis (Fig. 3) and was not seen in 3D7$^{\Delta Pfae3}$ parasite (Supplementary Fig. S4).
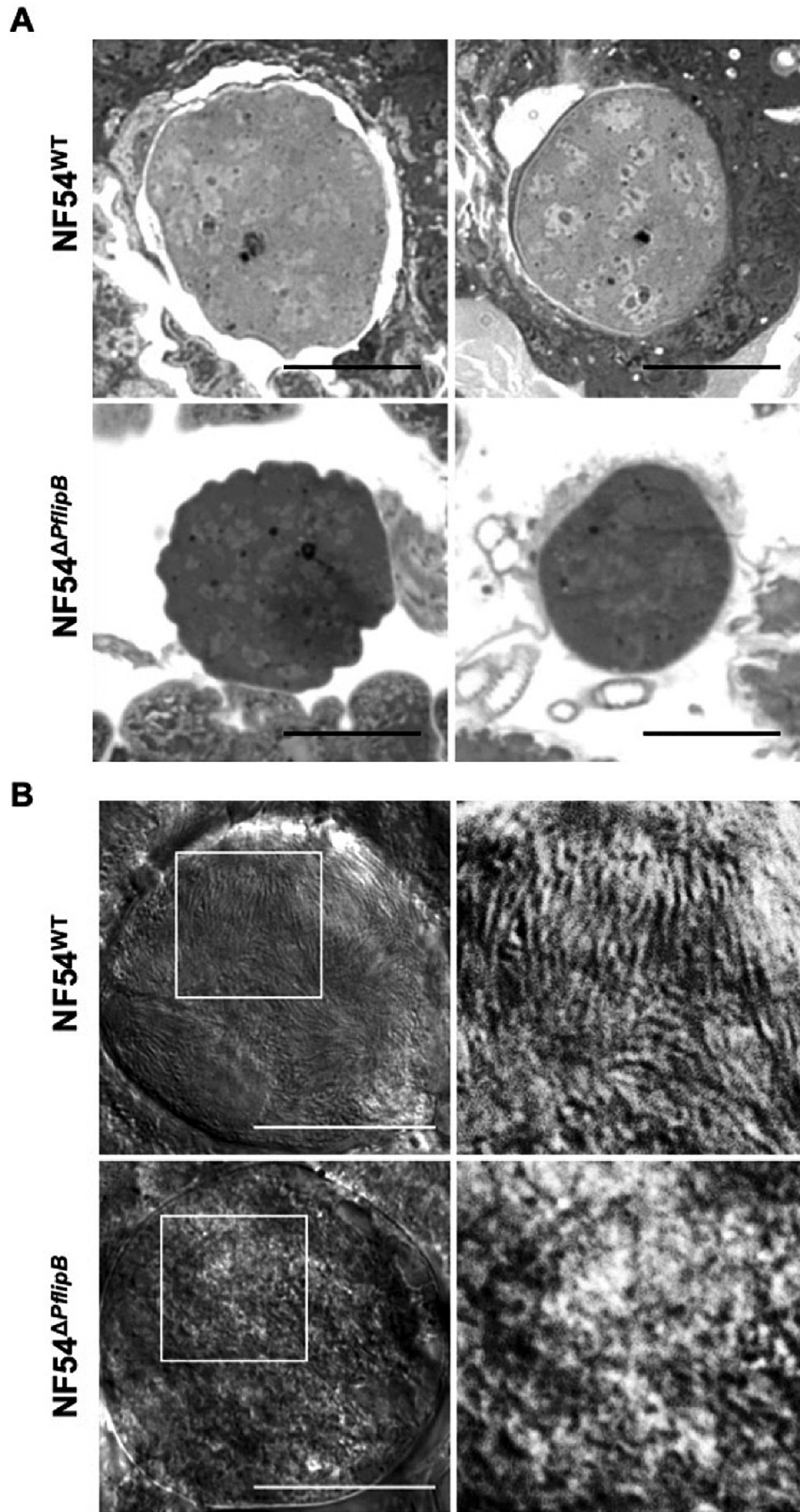
Fig. 7. *Plasmodium falciparum* oocyst morphology on days 7 and 13 post-feeding of gametocytes to *Anopheles* mosquitoes shows a defect in sporozoite development for lipoic acid protein ligase B (LipB) knockout parasites. (A) Two representative light microscopy images of NF54$^{\Delta lipB}$ and of NF54^{WT} oocytes on day 7 post-feeding. Scale bars = 25 microns (B) A representative differential interference contrast (DIC) microscopy image of NF54$^{\Delta lipB}$ and of NF54^{WT} oocytes on day 13. The insets are shown in white squares. Scale bar = 25 μm. The NF54$^{\Delta PflipB}$ oocysts show malformation in both methods and time points.

As it stands, these observations and the changes in redox regulators are linked to the deletion of *lipB*. However, we propose one possible model that could be considered for tying together the phenotypes of *lipB* deletion in the asexual stages: *lipB* deletion leads to LA depletion; changes to apicoplast redox balance due to this depletion of LA might induce changes in cytosolic redox through plastid-to-cytosol signalling as seen with other plastids. This putative signal leads to the temporary accelerated differentiation observed (Fig. 2C), which may be linked to the observed metabolic changes during the time window examined. Some uncertainty with this model stems from the potential dual roles of LA in (i) potentially regulating redox and (ii) supporting PDC-dependent fatty acid synthesis. However, accumulating evidence suggests that the latter is not essential during intra-erythrocytic development (Yeh and DeRisi, 2011; Cobbold et al., 2013) unless fatty acid starvation occurs (Botté et al., 2013). We thus propose that the changes in carbon metabolism observed upon *lipB* deletion are not the consequence of disruption of fatty acid metabolism. That said, we cannot rule out that the changes in cytosolic redox regulator expression, asexual cycle progression and the metabolic changes taking place in this mutant are not the cause of other outcomes of the *lipB* deletion not yet identified.

Plasmodium falciparum asexual blood stages are characterised by an oxidative TCA cycle, where the main carbon source is provided by 2-oxoglutarate that originates from glutamine. The majority of these glutamine-derived carbons exit the cycle as malate, while only a small fraction is further oxidised to generate oxaloacetate and citrate that then can take part again in the cycle (Cobbold et al., 2013; MacRae et al., 2013; Ke et al., 2015). Comparing the TCA cycle metabolism of 3D7$^{\Delta PflipB}$ mutants with 3D7^{WT} parasites revealed differences in the glucose-derived carbon input. In 3D7$^{\Delta PflipB}$ mutants, citrate presented mainly as M + 2 labelling and showed a significant decrease in M + 5 while all other isotopologues for this metabolite were below detection levels (Fig. 4D). These results suggest that citrate is likely mainly generated by unlabelled oxaloacetate that originated from anaplerotic unlabelled 2-oxoglutarate entering the TCA cycle and fully labelled pyruvate providing M + 2 acetyl-CoA (Fig. 4A). This observation and the apparent absence of M + 4 and M + 6 citrate isotopologues could suggest that that the small fraction of glucose-derived carbon is not taking part in the full cycle of 3D7$^{\Delta PflipB}$ mutants, unlike what happens in 3D7^{WT} parasites (Fig. 4D).

The link between *lipB* deletion and the changes seen in the TCA cycle requires further study, and the lack of change in ICDH protein levels (Fig. 5A, Supplementary Fig. S6) is puzzling. One possible explanation is that the enzymatic activity of ICDH, or indeed citrate synthase and aconitase, may be inhibited in response to the observed cellular redox changes. Studies on plant mitochondria highlight the role of thiol redox switches in adjusting mitochondrial function in light of external stresses (reviewed in Nietzel et al., 2017), and citrate synthase, aconitase and ICDH are all substrate for thiol based redox regulation (Yoshida et al., 2013; Schmidtmann et al., 2014; Yoshida and Hisabori, 2014).

Interestingly, alongside the altered levels of citrate labelling, we observed an increase in relative levels of BCKDH E2 (Fig. 5A) and no change in the total relative intracellular levels of citrate (Fig. 4B). Previous studies suggested that citrate could take part in a malate shuttle, whereby cytosolic citrate is used to generate oxaloacetate and acetyl-CoA, which in turn take part in carbon fixation and protein acetylation (Cobbold et al., 2013; Storm et al., 2014). The apparent absence of M + 4 and M + 6 citrate in 3D7$^{\Delta PflipB}$ mutants is in line with this scenario and could suggest that the citrate fraction that is not cycling in the TCA cycle but may instead be channelled towards this citrate shuttle. If true, this would result in increased availability of cytosolic acetyl-CoA, which in turn may affect histone acetylation and thus gene expression patterns

(Cobbold et al., 2016). Similarly, in macrophages activated by LPS and IFNγ, variations in the TCA cycle activity was observed along with reduced ICDH enzyme with consequent accumulation of citrate and succinate, generation of ROS signalling, and modulation of gene expression by alternative acetylation (Seim et al., 2019), lending precedence to our proposed explanation. This scenario remains, nonetheless, a speculative model that, if true, would explain the altered progression through the *P. falciparum* cell cycle, which typically depends on very tight regulation of gene expression (Bozdech et al., 2003).

We were unable to detect sporozoites in the salivary glands of mosquitoes infected with the NF54$^{\Delta Pflipb}$ mutant, despite the fact that normal numbers of oocysts were produced (Table 2, Fig. 6). This observation suggests that *lipB* is essential for successful sporogony. This finding is surprising considering the evidence from the rodent parasite *P. berghei*, where deletion of *lipB* caused no defect to the production of salivary gland sporozoites but showed a moderate defect in liver-stage development (Falkard et al., 2013). This is not the first example of such a discrepancy. PDC E1α is dispensable for mosquito development in the rodent malaria parasite *P. yoelii* but was necessary for sporozoite maturation in *P. falciparum* (Cobbold et al., 2013). These findings point to different dependencies of human and rodent malaria on PDC enzymes for development in the mosquito. A possible reason for this difference may be the increased number of sporozoites produced per oocyst, which is four-fold higher in the human malaria parasite *P. falciparum* (Rungsiwongse and Rosenberg, 1991) than in rodent malaria parasites (Lindner et al., 2013; Shimizu et al., 2010). High sporozoite numbers in rodent malaria oocysts may require enhanced metabolism, which would depend on both PDC activity and a functional redox regulation network. Future examination of the asexual stages of the NF54$^{\Delta Pflipb}$ mutant, such as the work presented here for the 3D7$^{\Delta PflipB}$ mutant, is merited to address the possibility that LA synthesis in the apicoplast is essential for completion of *P. falciparum* development in the mosquito vector.

Acknowledgements

Appendix A. Supplementary data

Supplementary data to this article can be found online at https://doi.org/10.1016/j.ijpara.2020.10.011.

References

Akide-Ndunge, O., Tambini, E., Giribaldi, G., McMillan, P.J., Müller, S., Arese, P., Turrini, F., 2009. Co-ordinated stage-dependent enhancement of *Plasmodium falciparum* antioxidant enzymes and heat shock protein expression in parasites growing in oxidatively stressed or G6PD-deficient red blood cells. Malar. J. 8, 113. https://doi.org/10.1186/1475-2875-8-113.

Becker, K., Tilley, L., Vennerstrom, J.L., Roberts, D., Rogerson, S., Ginsburg, H., 2004. Oxidative stress in malaria parasite-infected erythrocytes: Host-parasite interactions. Int. J. Parasitol. doi:10.1016/j.ijpara.2003.09.011.

Biddau, M., Bouchut, A., Major, J., Saveria, T., Tottey, J., Oka, O., Van-Lith, M., Jennings, K.E., Ovciarikova, J., DeRocher, A., Striepen, B., Waller, R.F., Parsons, M., Sheiner, L., 2018. Two essential Thioredoxins mediate apicoplast biogenesis, protein import, and gene expression in Toxoplasma gondii. PLoS Pathog. 14, e1006836. doi:10.1371/journal.ppat.1006836.

Biddau, M., Sheiner, L., 2019. Targeting the apicoplast in malaria. Biochem. Soc. Trans. 47, 973–983. https://doi.org/10.1042/BST20170563.

Bilska, A., Włodek, L., 2005. Lipoic acid - the drug of the future?. Pharmacol. Rep. 57, 570–577.

Bode, R., Ivanov, A.G., Hüner, N.P.A., 2016. Global transcriptome analyses provide evidence that chloroplast redox state contributes to intracellular as well as long-distance signalling in response to stress and acclimation in Arabidopsis. Photosynth. Res. 128, 287–312. https://doi.org/10.1007/s11120-016-0245-y.

Botte, C.Y., Yamaryo-Botte, Y., Rupasinghe, T.W.T., Mullin, K.A., MacRae, J.I., Spurck, T.P., Kalanon, M., Shears, M.J., Coppel, R.L., Crellin, P.K., Marechal, E., McConville, M.J., McFadden, G.I., 2013. Atypical lipid composition in the purified relict plastid (apicoplast) of malaria parasites. Proc. Natl. Acad. Sci. U. S. A. 110, 7506–7511. https://doi.org/10.1073/pnas.1301251110.

Boucher, M.J., Ghosh, S., Zhang, L., Lal, A., Jang, S.W., Ju, A., Zhang, S., Wang, X., Ralph, S.A., Zou, J., Elias, J.E., Yeh, E., 2018. Integrative proteomics and bioinformatic prediction enable a high-confidence apicoplast proteome in malaria parasites. PLoS Biol. 16, e2005895. doi:10.1371/journal.pbio.2005895.

Bozdech, Z., Llinás, M., Pulliam, B.L., Wong, E.D., Zhu, J., DeRisi, J.L., 2003. The transcriptome of the intraerythrocytic developmental cycle of Plasmodium falciparum. PLoS Biol. 1, E5. doi:10.1371/journal.pbio.0000005.

Bryk, R., Lima, C.D., Erdjument-Bromage, H., Tempst, P., Nathan, C., 2002. Metabolic enzymes of mycobacteria linked to antioxidant defense by a thioredoxin-like protein. Science 295, 1073–1077. https://doi.org/10.1126/science.1067798.

Bunik, V., Follmann, H., 1993. Thioredoxin reduction dependent on alpha-ketoacid oxidation by alpha-ketoacid dehydrogenase complexes. FEBS Lett. 336, 197–200. https://doi.org/10.1016/0014-5793(93)80801-Z.

Bushell, E., Gomes, A.R., Sanderson, T., Anar, B., Girling, G., Herd, C., Metcalf, T., Modrzynska, K., Schwach, F., Martin, R.E., Mather, M.W., McFadden, G.I., Parts, L., Rutledge, G.G., Vaidya, A.B., Wengelnik, K., Rayner, J.C., Billker, O., 2017. Functional profiling of a Plasmodium genome reveals an abundance of essential genes. Cell 170, 260–272.e8. https://doi.org/10.1016/j.cell.2017.06.030.

Chokkathukalam, A., Jankevics, A., Creek, D.J., Achcar, F., Barrett, M.P., Breitling, R., 2013. mzMatch-ISO: an R tool for the annotation and relative quantification of isotope-labelled mass spectrometry data. Bioinformatics 29, 281–283. https://doi.org/10.1093/bioinformatics/bts674.

Cobbold, S.A., Santos, J.M., Ochoa, A., Perlman, D.H., Llinás, M., 2016. Proteome-wide analysis reveals widespread lysine acetylation of major protein complexes in the malaria parasite. Sci. Rep. 6, 19722. https://doi.org/10.1038/srep19722.

Cobbold, S.A., Vaughan, A.M., Lewis, I.A., Painter, H.J., Camargo, N., Perlman, D.H., Fishbaugher, M., Healer, J., Cowman, A.F., Kappe, S.H.I., Llinás, M., 2013. Kinetic flux profiling elucidates two independent acetyl-CoA biosynthetic pathways in Plasmodium falciparum. J. Biol. Chem. 288, 36338–36350. https://doi.org/10.1074/jbc.M113.503557.

Crawford, M.J., Thomsen-Zieger, N., Ray, M., Schachtner, J., Roos, D.S., Seeber, F., 2006. Toxoplasma gondii scavenges host-derived lipoic acid despite its de novo synthesis in the apicoplast. EMBO J. 25, 3214–3222. https://doi.org/10.1038/sj.emboj.7601189.

Deponte, M., Becker, K., 2005. Glutathione S-transferase from malarial parasites: structural and functional aspects. Methods Enzymol. 401, 241–253. https://doi.org/10.1016/S0076-6879(05)01015-3.

Dietz, K.-J., Turkan, I., Krieger-Liszkay, A., 2016. Redox- and reactive oxygen species-dependent signaling into and out of the photosynthesizing chloroplast. Plant Physiol. 171, 1541–1550. https://doi.org/10.1104/pp.16.00375.

Dockrell, H.M., Playfair, J.H., 1984. Killing of Plasmodium yoelii by enzyme-induced products of the oxidative burst. Infect. Immun. 43, 451–456.

Falkard, B., Kumar, T.R.S., Hecht, L.-S., Matthews, K.A., Henrich, P.P., Gulati, S., Lewis, R.E., Manary, M.J., Winzeler, E.A., Sinnis, P., Prigge, S.T., Heussler, V., Deschermeier, C., Fidock, D., 2013. A key role for lipoic acid synthesis during Plasmodium liver stage development. Cell. Microbiol. 15, 1585–1604. https://doi.org/10.1111/cmi.12137.

Feeney, M.A., Veeravalli, K., Boyd, D., Gon, S., Faulkner, M.J., Georgiou, G., Beckwith, J., 2011. Repurposing lipoic acid changes electron flow in two important metabolic pathways of Escherichia coli. Proc. Natl. Acad. Sci. U. S. A. 108, 7991–7996. https://doi.org/10.1073/pnas.1105429108.

Foth, B.J., Stimmler, L.M., Handman, E., Crabb, B.S., Hodder, A.N., McFadden, G.I., 2005. The malaria parasite Plasmodium falciparum has only one pyruvate dehydrogenase complex, which is located in the apicoplast. Mol. Microbiol. 55, 39–53. https://doi.org/10.1111/j.1365-2958.2004.04407.x.

Frohnecke, N., Klein, S., Seeber, F., 2015. Protein-protein interaction studies provide evidence for electron transfer from ferredoxin to lipoic acid synthase in Toxoplasma gondii. FEBS Lett. 589, 31–36. https://doi.org/10.1016/j.febslet.2014.11.020.

Goodyer, I.D., Taraschi, T.F., 1997. Plasmodium falciparum: a simple, rapid method for detecting parasite clones in microtiter plates. Exp. Parasitol. 86, 158–160. https://doi.org/10.1006/expr.1997.4156.

Gorąca, A., Huk-Kolega, H., Piechota, A., Kleniewska, P., Ciejka, E., Skibska, B., 2011. Lipoic acid - biological activity and therapeutic potential. Pharmacol. Rep. 63, 849–858. https://doi.org/10.1016/S1734-1140(11)70600-4.

Graves, P.M., Carter, R., McNeill, K.M., 1984. Gametocyte production in cloned lines of Plasmodium falciparum. Am. J. Trop. Med. Hyg. 33, 1045–1050. https://doi.org/10.4269/ajtmh.1984.33.1045.

Günther, S., Storm, J., Müller, S., 2009. Plasmodium falciparum: organelle-specific acquisition of lipoic acid. Int. J. Biochem. Cell Biol. 41, 748–752. https://doi.org/10.1016/j.biocel.2008.10.028.

Günther, S., Wallace, L., Patzewitz, E.-M., McMillan, P.J., Storm, J., Wrenger, C., Bissett, R., Smith, T.K., Müller, S., 2007. Apicoplast lipoic acid protein ligase B is not essential for Plasmodium falciparum. PLoS Pathog. 3, e189. doi:10.1371/journal.ppat.0030189.

Haramaki, N., Han, D., Handelman, G.J., Tritschler, H.J., Packer, L., 1997. Cytosolic and mitochondrial systems for NADH- and NADPH-dependent reduction of alpha-lipoic acid. Free Radic. Biol. Med. 22, 535–542. https://doi.org/10.1016/S0891-5849(96)00400-5.

Harwaldt, P., Rahlfs, S., Becker, K., 2002. Glutathione S-transferase of the malarial parasite Plasmodium falciparum: characterization of a potential drug target. Biol. Chem. 383, 821–830. https://doi.org/10.1515/BC.2002.086.

Jankevics, A., Merlo, M.E., de Vries, M., Vonk, R.J., Takano, E., Breitling, R., 2012. Separating the wheat from the chaff: a prioritisation pipeline for the analysis of metabolomics datasets. Metabolomics 8, 29–36. https://doi.org/10.1007/s11306-011-0341-0.

Kagan, V.E., Shvedova, A., Serbinova, E., Khan, S., Swanson, C., Powell, R., Packer, L., 1992. Dihydrolipoic acid-a universal antioxidant both in the membrane and in the aqueous phase. Reduction of peroxyl, ascorbyl and chromanoxyl radicals. Biochem. Pharmacol. 44, 1637–1649. https://doi.org/10.1016/0006-2952(92)90482-X.

Ke, H., Lewis, I., Morrisey, J., McLean, K., Ganesan, S., Painter, H., Mather, M., Jacobs-Lorena, M., Llinás, M., Vaidya, A., 2015. Genetic investigation of tricarboxylic acid metabolism during the Plasmodium falciparum life cycle. Cell Rep. 11, 164–174. https://doi.org/10.1016/j.celrep.2015.03.011.

Kehr, S., Sturm, N., Rahlfs, S., Przyborski, J.M., Becker, K., 2010. Compartmentation of redox metabolism in malaria parasites. PLoS Pathog 6,. https://doi.org/10.1371/journal.ppat.1001242 e1001242.

Kimata-Ariga, Y., Yuasa, S., Saitoh, T., Fukuyama, H., Hase, T., 2018. Plasmodium-specific basic amino acid residues important for the interaction with ferredoxin on the surface of ferredoxin-NADP+ reductase. J. Biochem. 164, 231–237. https://doi.org/10.1093/jb/mvy045.

Krnajski, Z., Walter, R.D., Müller, S., 2001. Isolation and functional analysis of two thioredoxin peroxidases (peroxiredoxins) from Plasmodium falciparum. Mol. Biochem. Parasitol. 113, 303–308. https://doi.org/10.1016/S0166-6851(01)00219-5.

Laine, L.M., Biddau, M., Byron, O., Müller, S., 2015. Biochemical and structural characterization of the apicoplast dihydrolipoamide dehydrogenase of Plasmodium falciparum. Biosci. Rep. 35, 1–15. https://doi.org/10.1042/BSR20140150.

Lambros, C., Vanderberg, J.P., 1979. Synchronization of Plasmodium falciparum erythrocytic stages in culture. J. Parasitol. 65, 418–420. https://doi.org/10.2307/3280287.

Liebau, E., Bergmann, B., Campbell, A.M., Teesdale-Spittle, P., Brophy, P.M., Lüersen, K., Walter, R.D., 2002. The glutathione S-transferase from Plasmodium falciparum. Mol. Biochem. Parasitol. 124, 85–90. https://doi.org/10.1016/S0166-6851(02)00160-3.

Lim, L., McFadden, G.I., 2010. The evolution, metabolism and functions of the apicoplast. Philos. Trans. R. Soc. Lond. B. Biol. Sci. 365, 749–763. https://doi.org/10.1098/rstb.2009.0273.

Lindner, S.E., Mikolajczak, S.A., Vaughan, A.M., Moon, W., Joyce, B.R., Sullivan, W.J., Kappe, S.H.I., 2013. Perturbations of Plasmodium Puf2 expression and RNA-seq of Puf2-deficient sporozoites reveal a critical role in maintaining RNA homeostasis and parasite transmissibility. Cell. Microbiol. 15, 1266–1283. https://doi.org/10.1111/cmi.12116.

Livak, K.J., Schmittgen, T.D., 2001. Analysis of relative gene expression data using real-time quantitative PCR and the 2(-Delta Delta C(T)) Method. Methods 25, 402–408. https://doi.org/10.1006/meth.2001.1262.

MacRae, J.I., Dixon, M.W.A., Dearnley, M.K., Chua, H.H., Chambers, J.M., Kenny, S., Bottova, I., Tilley, L., McConville, M.J., 2013. Mitochondrial metabolism of sexual and asexual blood stages of the malaria parasite Plasmodium falciparum. BMC Biol. 11, 67. https://doi.org/10.1186/1741-7007-11-67.

Maier, A.G., Braks, J.A.M., Waters, A.P., Cowman, A.F., 2006. Negative selection using yeast cytosine deaminase/uracil phosphoribosyl transferase in Plasmodium falciparum for targeted gene deletion by double crossover recombination. Mol. Biochem. Parasitol. 150, 118–121. https://doi.org/10.1016/j.molbiopara.2006.06.014.

McMillan, P.J., Stimmler, L.M., Foth, B.J., McFadden, G.I., Müller, S., 2005. The human malaria parasite Plasmodium falciparum possesses two distinct dihydrolipoamide dehydrogenases. Mol. Microbiol. 55, 27–38. https://doi.org/10.1111/j.1365-2958.2004.04398.x.

Millard, P., Delépine, B., Guionnet, M., Heuillet, M., Bellvert, F., Létisse, F., Wren, J., 2019. IsoCor: Isotope correction for high-resolution MS labeling experiments. Bioinformatics 35, 4484–4487. https://doi.org/10.1093/bioinformatics/btz209.

Mohring, F., Pretzel, J., Jortzik, E., Becker, K., 2014. The redox systems of Plasmodium falciparum and Plasmodium vivax: comparison, in silico analyses and inhibitor studies. Curr. Med. Chem. 21, 1728–1756.

Mohring, F., Rahbari, M., Zechmann, B., Rahlfs, S., Przyborski, J.M., Meyer, A.J., Becker, K., 2017. Determination of glutathione redox potential and pH value in subcellular compartments of malaria parasites. Free Radic. Biol. Med. 104, 104–117. https://doi.org/10.1016/j.freeradbiomed.2017.01.001.

Mooney, B.P., Miernyk, J.A., Randall, D.D., 2002. The complex fate of alpha-ketoacids. Annu. Rev. Plant Biol. 53, 357–375. https://doi.org/10.1146/annurev.arplant.53.100301.135251.

Moura, F.A., de Andrade, K.Q., dos Santos, J.C.F., Goulart, M.O.F., 2015. Lipoic Acid: its antioxidant and anti-inflammatory role and clinical applications. Curr. Top. Med. Chem. 15, 458–483. https://doi.org/10.2174/1568026615666150114161358.

Müller, S., 2015. Role and regulation of glutathione metabolism in *Plasmodium falciparum*. Molecules 20, 10511–10534. https://doi.org/10.3390/molecules200610511.

Nepveu, F., Turrini, F., 2013. Targeting the redox metabolism of *Plasmodium falciparum*. Future Med. Chem. https://doi.org/10.4155/fmc.13.159.

Nietzel, T., Mostertz, J., Hochgräfe, F., Schwarzländer, M., 2017. Redox regulation of mitochondrial proteins and proteomes by cysteine thiol switches. Mitochondrion 33, 72–83. https://doi.org/10.1016/j.mito.2016.07.010.

O'Neill, M.T., Phuong, T., Healer, J., Richard, D., Cowman, A.F., O'Neill, M.T., Phuong, T., Healer, J., Richard, D., Cowman, A.F., 2011. Gene deletion from *Plasmodium falciparum* using FLP and Cre recombinases: Implications for applied site-specific recombination. Int. J. Parasitol. 41, 117–123.

Oppenheim, R.D., Creek, D.J., Macrae, J.I., Modrzynska, K.K., Pino, P., Limenitakis, J., Polonais, V., Seeber, F., Barrett, M.P., Billker, O., McConville, M.J., Soldati-Favre, D., 2014. BCKDH: The missing link in apicomplexan mitochondrial metabolism is required for full virulence of Toxoplasma gondii and Plasmodium berghei. PLoS Pathog. doi:10.1371/journal.ppat.1004263.

Packer, L., Witt, E.H., Tritschler, H.J., 1995. alpha-Lipoic acid as a biological antioxidant. Free Radic. Biol. Med. 19, 227–250. https://doi.org/10.1016/0891-5849(95)00017-R.

Patzewitz, E.-M., Salcedo-Sora, J.E., Wong, E.H., Sethia, S., Stocks, P.A., Maughan, S.C., Murray, J.A.H., Krishna, S., Bray, P.G., Ward, S.A., Müller, S., 2013. Glutathione transport: a new role for pfcrt in chloroquine resistance. Antioxid. Redox Signal. https://doi.org/10.1089/ars.2012.4625.

Perham, R.N., 2000. Swinging arms and swinging domains in multifunctional enzymes: catalytic machines for multistep reactions. Annu. Rev. Biochem. 69, 961–1004. https://doi.org/10.1146/annurev.biochem.69.1.961.

Pick, U., Haramaki, N., Constantinescu, A., Handelman, G.J., Tritschler, H.J., Packer, L., 1995. Glutathione reductase and lipoamide dehydrogenase have opposite stereospecificities for alpha-lipoic acid enantiomers. Biochem. Biophys. Res. Commun. 206, 724–730. https://doi.org/10.1006/bbrc.1995.1102.

Ponnudurai, T., Lensen, A.H.W., Meis, J.F.G.M., Meuwissen, J.H.E., 1986. Synchronization of *Plasmodium falciparum* gametocytes using an automated suspension culture system. Parasitology 93, 263–274. https://doi.org/10.1017/S003118200005143X.

Rungsiwongse, J., Rosenberg, R., 1991. The number of sporozoites produced by individual malaria oocysts. Am. J. Trop. Med. Hyg. 45, 574–577. https://doi.org/10.4269/ajtmh.1991.45.574.

Salcedo-Sora, J.E., Caamano-Gutierrez, E., Ward, S.A., Biagini, G.A., 2014. The proliferating cell hypothesis: a metabolic framework for *Plasmodium* growth and development. Trends Parasitol 30, 170–175. https://doi.org/10.1016/j.pt.2014.02.001.

Scheltema, R.A., Jankevics, A., Jansen, R.C., Swertz, M.A., Breitling, R., 2011. PeakML/mzMatch: a file format, Java library, R library, and tool-chain for mass spectrometry data analysis. Anal. Chem. 83, 2786–2793. https://doi.org/10.1021/ac2000994.

Schmidtmann, E., König, A.-C., Orwat, A., Leister, D., Hartl, M., Finkemeier, I., 2014. Redox regulation of *Arabidopsis* mitochondrial citrate synthase. Mol. Plant 7, 156–169. https://doi.org/10.1093/mp/sst144.

Seeber, F., Aliverti, A., Zanetti, G., 2005. The plant-type ferredoxin-NADP+ reductase/ferredoxin redox system as a possible drug target against apicomplexan human parasites. Curr. Pharm. Des. 11, 3159–3172. https://doi.org/10.2174/1381612054864957.

Seeber, F., Soldati-Favre, D., 2010. Metabolic pathways in the apicoplast of apicomplexa. Int. Rev. Cell Mol. Biol. 281, 161–228. https://doi.org/10.1016/S1937-6448(10)81005-6.

Sewelam, N., Jaspert, N., Van Der Kelen, K., Tognetti, V.B., Schmitz, J., Frerigmann, H., Stahl, E., Zeier, J., Van Breusegem, F., Maurino, V.G., 2014. Spatial H2O2 signaling specificity: H2O2 from chloroplasts and peroxisomes modulates the plant transcriptome differentially. Mol. Plant 7, 1191–1210. https://doi.org/10.1093/mp/ssu070.

Sheiner, L., Vaidya, A.B., McFadden, G.I., 2013. The metabolic roles of the endosymbiotic organelles of *Toxoplasma* and *Plasmodium* spp. Curr. Opin. Microbiol. 16, 452–458. https://doi.org/10.1016/j.mib.2013.07.003.

Shimizu, S., Osada, Y., Kanazawa, T., Tanaka, Y., Arai, M., 2010. Suppressive effect of azithromycin on Plasmodium berghei mosquito stage development and apicoplast replication. doi:10.1186/1475-2875-9-73.

Shivapurkar, R., Hingamire, T., Kulkarni, A.S., Rajamohanan, P.R., Reddy, D.S., Shanmugam, D., 2018. Evaluating antimalarial efficacy by tracking glycolysis in *Plasmodium falciparum* using NMR spectroscopy. Sci. Rep. 8, 1–10. https://doi.org/10.1038/s41598-018-36197-3.

Siciliano, G., Santha Kumar, T.R., Bona, R., Camarda, G., Calabretta, M.M., Cevenini, L., Davioud-Charvet, E., Becker, K., Cara, A., Fidock, D.A., Alano, P., 2017. A high susceptibility to redox imbalance of the transmissible stages of *Plasmodium falciparum* revealed with a luciferase-based mature gametocyte assay. Mol. Microbiol. 104, 306–318. https://doi.org/10.1111/mmi.13626.

Storm, J., Sethia, S., Blackburn, G.J., Chokkathukalam, A., Watson, D.G., Breitling, R., Coombs, G.H., Müller, S., 2014. Phosphoenolpyruvate carboxylase identified as a key enzyme in erythrocytic Plasmodium falciparum carbon metabolism. PLoS Pathog. 10, e1003876. doi:10.1371/journal.ppat.1003876.

Sumner, L.W., Amberg, A., Barrett, D., Beale, M.H., Beger, R., Daykin, C.A., Fan, T.-M., Fiehn, O., Goodacre, R., Griffin, J.L., Hankemeier, T., Hardy, N., Harnly, J., Higashi, R., Kopka, J., Lane, A.N., Lindon, J.C., Marriott, P., Nicholls, A.W., Reily, M.D., Thaden, J.J., Viant, M.R., 2007. Proposed minimum reporting standards for chemical analysis: Chemical Analysis Working Group (CAWG) Metabolomics Standards Initiative (MSI). Metabolomics 3, 211–221. https://doi.org/10.1007/s11306-007-0082-2.

Tautenhahn, R., Böttcher, C., Neumann, S., 2008. Highly sensitive feature detection for high resolution LC/MS. BMC Bioinformatics 9. https://doi.org/10.1186/1471-2105-9-504.

Tibullo, D., Li Volti, G., Giallongo, C., Grasso, S., Tomassoni, D., Anfuso, C.D., Lupo, G., Amenta, F., Avola, R., Bramanti, V., 2017. Biochemical and clinical relevance of alpha lipoic acid: antioxidant and anti-inflammatory activity, molecular pathways and therapeutic potential. Inflamm. Res. 66, 947–959. https://doi.org/10.1007/s00011-017-1079-6.

Trager, W., Jensen, J.B., 1976. Human malaria parasites in continuous culture. Science 193, 673–675. https://doi.org/10.1038/098448b0.

Urscher, M., Przyborski, J.M., Imoto, M., Deponte, M., 2010. Distinct subcellular localization in the cytosol and apicoplast, unexpected dimerization and inhibition of *Plasmodium falciparum* glyoxalases. Mol. Microbiol. 76, 92–103. https://doi.org/10.1111/j.1365-2958.2010.07082.x.

Vaughan, A.M., O'Neill, M.T., Tarun, A.S., Camargo, N., Phuong, T.M., Aly, A.S.I., Cowman, A.F., Kappe, S.H.I., 2009. Type II fatty acid synthesis is essential only for malaria parasite late liver stage development. Cell. Microbiol. 11, 506–520. https://doi.org/10.1111/j.1462-5822.2008.01270.x.

Vincent, I.M., Barrett, M.P., 2015. Metabolomic-based strategies for anti-parasite drug discovery. J. Biomol. Screen. 20, 44–55. https://doi.org/10.1177/1087057114551519.

Wezena, C.A., Alisch, R., Golzmann, A., Liedgens, L., Staudacher, V., Pradel, G., Deponte, M., 2017. The cytosolic glyoxalases of *Plasmodium falciparum* are dispensable during asexual blood-stage development. Microb. cell (Graz , Austria) 5, 32–41. https://doi.org/10.15698/mic2018.01.608.

World Health Organization, 2019. World Malaria Report 2019. Geneva.

Yhe, E., DeRisi, JL., Chemical rescue of malaria parasites lacking an apicoplast defines organelle function in blood-stage Plasmodium Falciparum. PLoS Biol. 2011;9(8):e1001138. doi: 10.1371/journal.pbio.1001138.

Yoshida, K., Hisabori, T., 2014. Mitochondrial isocitrate dehydrogenase is inactivated upon oxidation and reactivated by thioredoxin-dependent reduction in *Arabidopsis*. Front. Environ. Sci. 2, 1–7. https://doi.org/10.3389/fenvs.2014.00038.

Yoshida, K., Noguchi, K., Motohashi, K., Hisabori, T., 2013. Systematic exploration of thioredoxin target proteins in plant mitochondria. Plant Cell Physiol. https://doi.org/10.1093/pcp/pct037.

Zhang, M., Wang, C., Otto, T.D., Oberstaller, J., Liao, X., Adapa, S.R., Udenze, K., Bronner, I.F., Casandra, D., Mayho, M., Brown, J., Li, S., Swanson, J., Rayner, J.C., Jiang, R.H.Y., Adams, J.H., 2018. Uncovering the essential genes of the human malaria parasite *Plasmodium falciparum* by saturation mutagenesis. Science 360, eaap7847. https://doi.org/10.1126/science:aap7847.

Zocher, K., Fritz-Wolf, K., Kehr, S., Fischer, M., Rahlfs, S., Becker, K., 2012. Biochemical and structural characterization of *Plasmodium falciparum* glutamate dehydrogenase 2. Mol. Biochem. Parasitol. 183, 52–62. https://doi.org/10.1016/j.molbiopara.2012.01.007.

Zuzarte-Luís, V., Mello-Vieira, J., Marreiros, I.M., Liehl, P., Chora, Â.F., Carret, C.K., Carvalho, T., Mota, M.M., 2017. Dietary alterations modulate susceptibility to *Plasmodium* infection. Nat. Microbiol. 2, 1600–1607. https://doi.org/10.1038/s41564-017-0025-2.